ELSEVIER

Atmospheric Research 45 (1998) 275–297

ATMOSPHERIC RESEARCH

Development of giant drops and high-reflectivity cores in Hawaiian clouds: numerical simulations using a kinematic model with detailed microphysics

Tamir G. Reisin, Yan Yin, Zev Levin *, Shalva Tzivion

Department of Geophysics and Planetary Sciences, Raymond and Beverly Sackler Faculty of Exact Sciences, Tel Aviv University, Ramat Aviv 69978, Israel

Received 6 January 1997; accepted 9 October 1997

Abstract

Cores of high radar reflectivity (>50 dBZ) and raindrops larger than 4 mm in diameter were occasionally reported in warm clouds, offshore from Hawaii. A kinematic numerical model with detailed microphysics was used to study the formation of these cores and the development of the giant drops. The role of collisional and spontaneous breakup of drops was evaluated. Our results show that spontaneous breakup of raindrops restricts the formation of giant drops ($D>4$ mm). This could be a result of the poor parameterization of the fragment size distribution, and the probabilities of the spontaneous breakup. The inclusion of only binary breakup mechanism explained the observed radar echoes and the drop spectra. These results corroborate the hypothesis that the updrafts in the Hawaiian clouds sort out different size drops in such a way that millimeter size drops are allowed to fall in an environment deficient of smaller raindrops. In this way, the large raindrops continue to grow by collection of small cloud droplets, but have a smaller chance for collisional breakup (the efficiency for this type of breakup is small for collisions with cloud droplets). The collisional breakup of big raindrops was also found to play a significant role in the formation of giant drops. Such drops are formed following collision–breakup of large raindrops in which one of the fragments is larger than the original drops. © 1998 Elsevier Science B.V.

Keywords: Cloud modeling; Warm rain; Breakup of drops

* Corresponding author. Fax: +972-3-6408274; e-mail: zev@hail.tau.ac.il

PII S0169-8095(97)00081-1

1. Introduction

Hawaiian clouds have been widely recognized as typical examples for rain production by warm processes. Warm temperatures, aerosol concentrations and other environmental conditions lead to the development of maritime, shallow convective clouds without any ice but with copious amounts of rain.

Although Hawaiian clouds have been extensively measured (e.g., Lavoie, 1967; Rogers, 1967; Takahashi et al., 1989) and modeled (Takahashi, 1981; Smolarkiewicz et al., 1988), inconsistencies appear between the observations and model results, especially with respect to microphysical parameters. Observations (Beard et al., 1986; Rauber et al., 1991) reported the development of high-reflectivity cores within 30 min from cloud formation and drops larger than 4 mm in diameter (and up to 8 mm) were relatively frequently measured. Although multidimensional models succeeded to realistically simulate the dynamical behavior of the cloud systems, they failed to simulate the fast formation of rain and the formation of drops larger than 4 mm (Pontikis et al., 1987).

The most comprehensive observational work to date on the development of high-reflectivity cores and the formation of giant drops, that includes both radar and microphysical data is the one by Szumowski et al. (1997a,b). In these works, radar data is correlated with the dynamics of the cloud and with microphysical data.

It is known that drops grow by condensation and collection, and the appearance of giant drops is limited by drop breakup. Drops can shatter due to self-breakup (also called spontaneous) or following collisions (called binary breakup). In this work, the term giant drops is used to represent drops larger than 4 mm in diameter.

Spontaneous breakup seems to occur very rarely in nature. Komabayasi et al. (1964) measurements were conducted under conditions that do not apply to atmospheric processes (Pruppacher and Klett, 1997). Rogers and Yau (1989) summarize that water drops can reach sizes much larger than those stated by Komabayasi before they disintegrate, and that this process can be considered unimportant in the development of raindrop spectra in the atmosphere. The use of the numerical formulation for spontaneous breakup by Srivastava (1971) (based on Komabayasi's measurements) severely restricts the existence of large drops while exaggerating the number of fragments produced. In spite of this, most of the numerical models in use (e.g., Takahashi, 1981; Kogan, 1991) still include spontaneous breakup of drops as the only breakup mechanism.

Binary breakup seems to be the relevant process that controls the formation and annihilation of big raindrops in nature. Szumowski et al. (1997b) hypothesize that binary breakup is the process responsible for the formation of giant drops in Hawaiian clouds.

In order to investigate the development of high reflectivity cores and the development of giant drops in Hawaiian clouds, we used a prescribed kinematic flow model and coupled it with the microphysical processes formulated using the accurate multi-moment method (Tzivion et al., 1987). The kinematic model resembled the observations of development of intense cells off the shore of Hawaii, on 10 August 1990. Since the aim of this investigation was to understand the role of drop growth and breakup on the development of giant drops, simulations were carried out using different drop breakup schemes such as spontaneous and binary. These two processes were used separately and

together to identify the most prominent mechanism responsible for the production (or annihilation) of the giant drops. Similarly, the results of using these different mechanisms were evaluated for their ability to mimic the development of precipitation and the history of the radar reflectivity. We show that by using a relatively accurate numerical method for solving the microphysical processes (multi-moments method) and by introducing binary breakup, we can adequately simulate the formation of rain and of giant drops, in harmony with the observations. The inclusion of spontaneous breakup is shown to lead to results that do not resemble the measurements.

2. Model description

The microphysical processes introduced in the kinematic model were formulated according to the multi-moments method (Tzivion et al., 1987) and will be briefly described here. For a more detailed description of the model, see Tzivion et al. (1994). The microphysical processes included were: drops nucleation, condensation/evaporation, collision–coalescence, binary breakup and spontaneous breakup. Sedimentation was present in the kinematic model.

The temporal changes in the drop size distribution function $n(m,t)$ with respect to mass m, at time t, due to microphysical processes can be written as (a dependence on some spatial dimension was implicitly assumed):

$$\frac{\partial n(m,t)}{\partial t} = \frac{\delta n(m,t)}{\delta t}\Big|_{\text{nucleation}} + \frac{\delta n(m,t)}{\delta t}\Big|_{\text{condensation/evaporation}} + \frac{\delta n(m,t)}{\delta t}\Big|_{\text{collision/breakup}} + \frac{\delta n(m,t)}{\delta t}\Big|_{\text{spontaneousbreakup}} \quad (1)$$

In the simulations, the drop spectrum was divided into 34 bins (x_k, $k=1,\ldots,34$) with mass doubling in each bin ($x_{k+1}=2x_k$) with a minimum diameter of 3.125 μm and a maximum of 8064 μm. By applying the operator $\int_{x_k}^{x_{k+1}} m^j \mathrm{d}m$ to both sides of Eq. (1), a set of equations for moments of the distribution function in each bin was obtained. We solved for the first two moments, N_k and M_k, the number and mass concentrations, respectively, in bin k:

$$N_k(t) = \int_{x_k}^{x_{k+1}} n_k(m,t)\mathrm{d}m \quad (2)$$

$$M_k(t) = \int_{x_k}^{x_{k+1}} m n_k(m,t)\mathrm{d}m \quad (3)$$

The radar reflectivity in bin k was calculated using the non-dimensional parameter ξ that relates between three consecutive moments (for details see Tzivion et al., 1987):

$$Z_k(t) = \xi \frac{M_k^2(t)}{N_k(t)} \quad (4)$$

and the total radar reflectivity was given by:

$$Z(t) = \sum_{k=1}^{k_{\max}} Z_k(t) \quad (5)$$

The activation of cloud condensation nuclei (CCN) was parameterized according to the activation spectra provided by Szumowski et al. (1998), characteristic to Hawaiian clouds. At each time step, the total number of CCN, N_{CCN}, that can be activated according to the supersaturation S and the activation spectra, was calculated and compared with the number of previously activated nuclei, N_{act}. If N_{act} was greater than N_{CCN}, no nucleation was performed; otherwise ($N_{CCN} - N_{act}$) new droplets were created. Since in a convective cloud, the initial growth of the activated CCN is very fast, we assumed that within one time step they become droplets. The newborn droplets were then distributed in two possible ways: they were all inserted in one bin (usually the first bin with an average mass at the middle of the bin) or they were distributed using a predetermined complete gamma distribution function:

$$f(r) = A\bar{r}^{\beta}e^{-B\bar{r}^{\gamma}} \tag{6}$$

where β and γ are parameters. A and B are functions of β, γ and $\bar{r}$ (the average radius of the nucleated droplets).

The condensation/evaporation process was solved using the method proposed by Tzivion et al. (1989) with modifications introduced by Stevens et al. (1996). In this approach, the differential equation for the rate of change of the distribution function due to condensation/evaporation was solved analytically for one time step, and the variation in the supersaturation during the time step was evaluated.

The solution to the stochastic equation for collisional coalescence/breakup equation was given by Tzivion et al. (1987) and Feingold et al. (1988). The collection and breakup kernels were according to Low and List (1982a,b), Ochs et al. (1986) and Long (1974) for drop size larger than 0.6 mm, 0.1–0.6 mm and smaller than 0.1 mm, respectively.

Spontaneous breakup was introduced using Komabayasi et al. (1964) probability function and the parameterization by Srivastava (1971) for the fragment distribution. An interesting, probably wrong, feature of this parameterization is the constant total number of fragments (62.2) and its independence of the mass of the parent drop, namely:

$$\int_0^m Q(x,m)\,\mathrm{d}x = 62.2 \tag{7}$$

where $Q(x,m)$ is the distribution function of the fragments as defined by Srivastava (1971):

$$Q(x,m) = \frac{145.37}{x}\,\frac{r_x}{r_m}e^{-7\frac{r_x}{r_m}},\ x \le m, \tag{8}$$

m represents the mass of the parent drop and x the fragments' mass, r_m and r_x are the respective radii. Srivastava's formula conserves the mass of the parent drop, but it cannot distinguish between the number of fragments produced by a small raindrop from those produced by a large one. This is in some disagreement with the Komabayasi et al.'s experimental data that showed that the number of fragments from different size drops could differ by more than one order of magnitude.

Terminal velocities of drops were calculated according to Beard (1977) as

$$v(m) \to v_k = \alpha_k \overline{m}_k^{\beta_k} \tag{9}$$

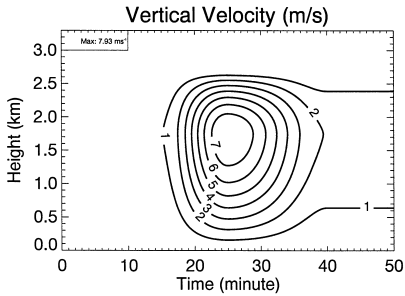

Fig. 1. Vertical velocity at the center of the domain as a function of height and time.

where v_k is the terminal velocity in bin k, $\overline{m}_k$ is the average mass in bin k and (α,β) are drop mass-dependent parameters.

The time step used in all the calculations was 3 s.

3. The kinematic model

The kinematic model prescribed an evolving flow and performed 2D advection of the temperature and water variables. A detailed description of the model is given by Szumowski et al. (1998). The model solved for the potential temperature, water vapor mixing ratio, mixing ratio for condensed water, and in our case also for number concentration of drops and activated CCN. The total number of microphysical variables was $34 \times 2 + 1 = 69$.

The model domain was 9 km in the horizontal and 3 km in the vertical, the grid size was 50 m in both directions. In the simulation, the cloud developed in the middle of the domain. The flow field for the simulation was constructed in a 2D flow characteristics based on dual-Doppler analysis of cloud-relative flow through intense cells that developed on 10 August 1990 off the windward shore of Hawaii. Fig. 1 displays the results from the kinematic flow model of the vertical velocity in the middle of the domain as a function of time. Until 15 min of simulation the updrafts were weaker than 1 m s^{-1}, afterwards they increased very rapidly reaching a maximum of 8 m s^{-1} some 10 min later. These strong updrafts (> 7 m s^{-1}) lasted for approximately 8–9 min in a region 1.3 to 2.1 km height. After 40 min, the maximum updraft decreased to below 2 m s^{-1}. The entire test simulated 50 min of real time, in which the cloud developed, produced rain and decayed. No downdrafts were included in the kinematic model since no discernible ones were detected in the observations.

4. Results

A number of simulations were conducted in order to evaluate the influence of the different breakup mechanisms on the evolution of the drop spectra and the role of the

Table 1
List of simulations conducted

Case	Nucleation	β	γ	$\bar{r}$ (μm)	Binary breakup	Spontaneous breakup
Reference	γ	2	1	11	✓	–
A	Bin 1	NA	NA	1.8	✓	–
B	γ	2	1	7	✓	–
C	γ	2	1	11	✓	✓
D	γ	2	1	11	–	✓
E	γ	2	1	11	–	–

initial cloud drop distribution on the subsequent evolution of the microphysical processes.

For comparison between the different simulations, we chose a reference case in which only binary breakup is considered, and the initial drop spectrum was represented

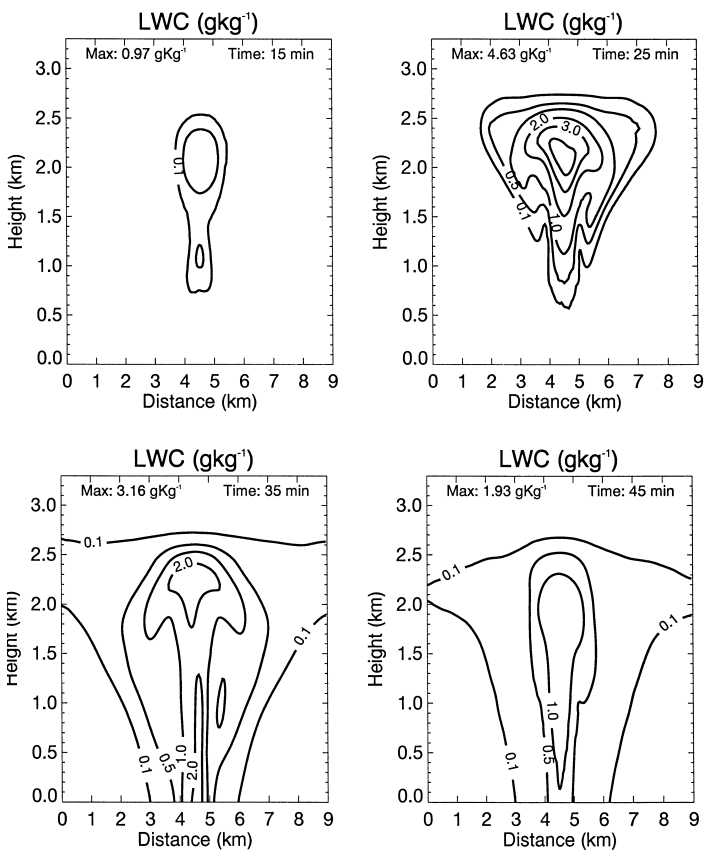

Fig. 2. Contours of LWC at four different times during the lifetime of the cloud.

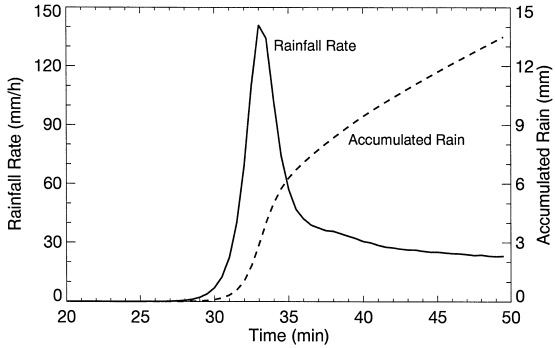

Fig. 3. Time variation of rainfall rate and accumulated rain at the center of the domain.

by a broad gamma function with parameters: $\beta = 2$, $\gamma = 1$ and $\bar{r} = 11$ μm. All the simulations conducted are defined in Table 1.

After 10 min of simulation, the cloud began to develop and 5 min later, the maximum liquid water content, LWC, was almost 1 g kg^{-1}. Fig. 2 shows contours of LWC at four different times during the simulation. After 25 min, the cloud reached its maximum development with a maximum LWC of 4.63 g kg^{-1}. At this stage, cloud base (defined by 100% relative humidity) was located at a height of 900 m and cloud top (similar definition) at 2800 m height. Rainfall rate and accumulated rain at the center of the domain are plotted in Fig. 3. Significant rainfall (> 10 mm h^{-1}) reached the ground after 30 min of simulation, reaching a maximum of about 140 mm h^{-1} 3 min later. Afterwards, the rain rate sharply decreased to 40 mm h^{-1} at 35 min, but from then on it continued to decrease slowly, and 10 min later the rainfall rate was still about 30 mm h^{-1}. By the end of the simulation, about 13.5 mm of rain accumulated in the center of the domain.

Fig. 4 shows the radar reflectivity as a function of time, averaged over 50 m, at the center of the domain. Echoes of 10 dBZ appeared at a height of 2 km after 15 min of simulation. At that location, the LWC was ≈ 1 g kg^{-1} (see Fig. 2). Following that, the

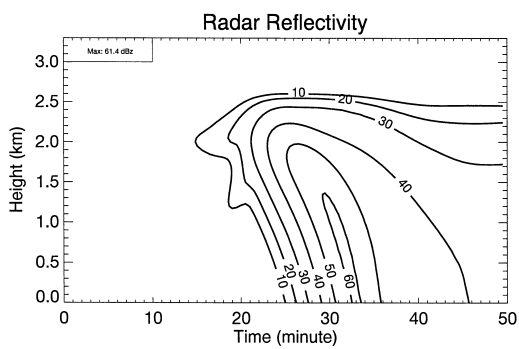

Fig. 4. Radar reflectivity (in dBZ) as a function of time and height, averaged over 50 m, at the center of the domain.

radar reflectivity increased very fast, and within 10 min a core of high reflectivity (>50 dBZ) appeared at a height of 1750 m. The maximum reflectivity obtained in the simulation was 61.4 dBZ, just below cloud base, 32.5 min from model initiation. As already pointed out with respect to the LWC, the decay of the cloud was relatively slow, maintaining echoes of more than 30 dBZ from about 1800 m down to the ground. This result stems from the fact that in the kinematic model, no downdrafts were allowed to develop, but instead maintained an updraft larger than 1 m s^{-1} until the end of the simulation. This updraft permitted raindrops to form, producing the simulated radar reflectivities.

Fig. 5a and b present contours of radar reflectivity every 2.5 min around the time of the development of the high-reflectivity core. At 22.5 min of cloud simulation, maximum reflectivity of 35.6 dBZ already appeared at about 2 km height. Two and a half minutes later, the very first raindrops began reaching the ground. Although the mass and

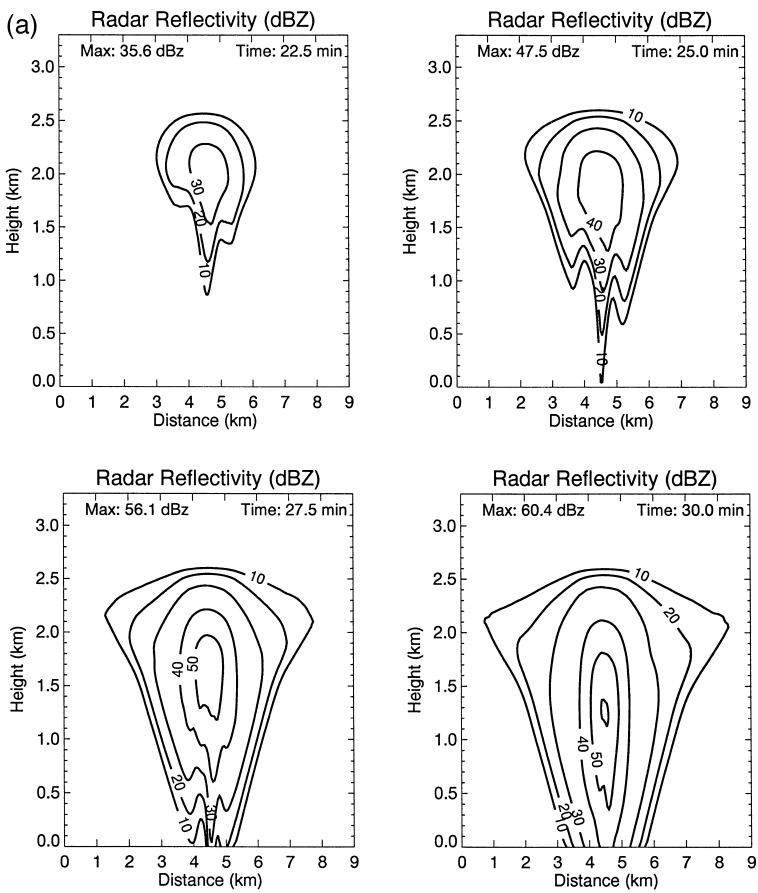

Fig. 5. (a) Contours of radar reflectivity at 22.5, 25, 27.5 and 30 min of cloud simulation. (b) Contours of radar reflectivity at 32.5, 35, 37.5 and 40 min of cloud simulation.

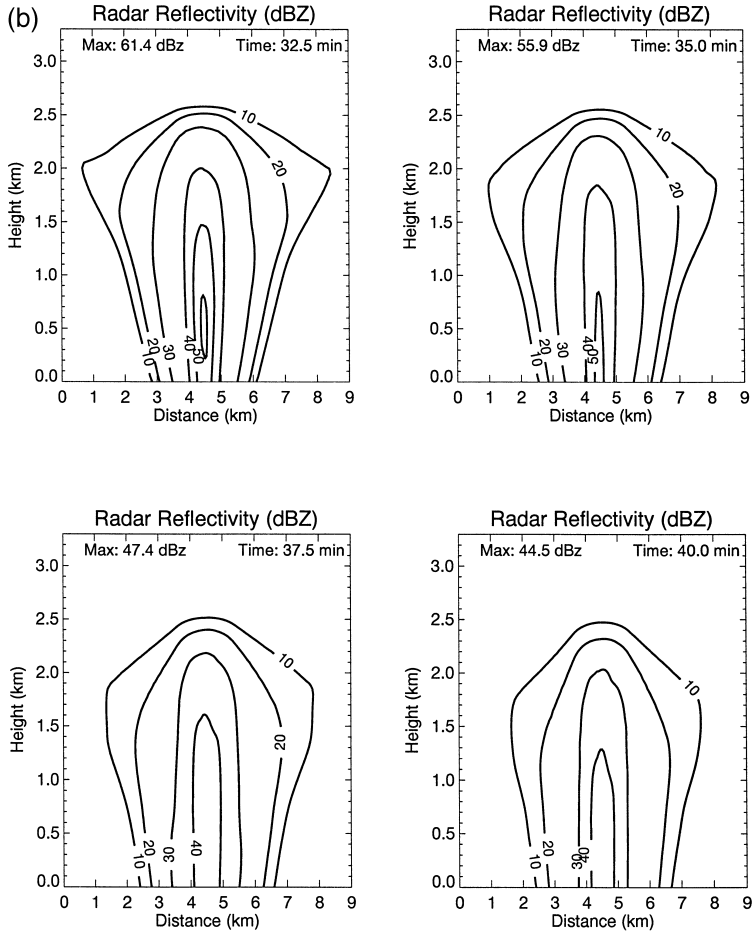

Fig. 5 (continued).

number of these drops were extremely low, they were large enough to produce an echo greater than 5 dBZ. The radar reflectivity continued to increase, reaching a value of 56.1 dBZ at around 1.6 km. This high value was a result of the increased size of the largest drops due to collection of smaller ones rising in the updraft. What we see here is first levitation of large drops followed by their sedimentation due to their continual growth. At 30 min of simulation, a maximum reflectivity of 60.4 dBZ appeared at 1250 m height near the center of the domain; the 50 dBZ contour stretched for almost 1500 m between 300 to 1800 m height. This core of high reflectivity was relatively narrow, less than 1 km wide.

Maximum radar reflectivity was obtained 2.5 min later (32.5 min) just below cloud base with a value of 61.4 dBZ. In Fig. 5b, contours of radar reflectivity are shown from 32.5 to 40 min depicting the decay stage of the cloud. As already pointed out, this stage continued until the end of the simulation with radar echoes slowly decreasing. Fig. 5

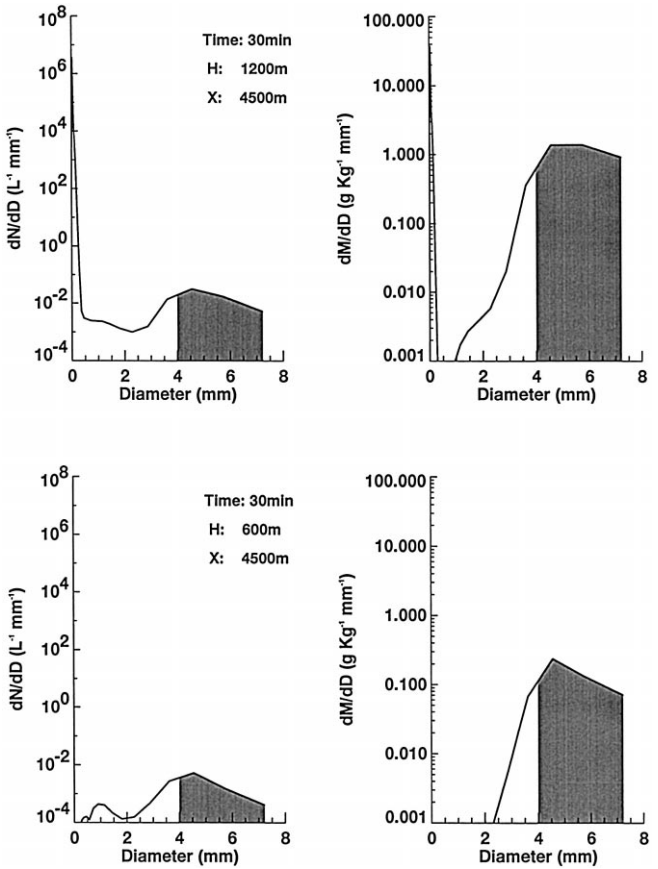

Fig. 6. Size distributions by number and mass, 30 min from model initiation at the center of the domain, at a height of 600 m (lower graphs) and 1200 m (upper graphs).

shows that the radar reflectivity distributions at 37.5 and 40 min were very similar, with the maximum value varying by only 3 dBZ.

The number and mass distribution functions of the drops at different locations and times are shown in Figs. 6–9. The shaded areas represent giant drops (>4 mm in diameter). Fig. 6 shows the distributions functions at the center of the domain, 30 min from model initiation, 300 m below cloud base (600 m) and 300 m above (1200 m). The distributions at 1200 m almost coincided with the location of the highest radar reflectivity (see Fig. 5a) which was 59.7 dBZ. Giant drops, in concentrations of 33 m^{-3}, were present at that location and they contributed $\approx 70\%$ of the LWC. Evaporation below cloud base affected the mass of all the raindrops, but it almost completely depleted the smaller drops. Fig. 7 presents the drop distribution functions at 1800 and 2400 m height. The maximum number and mass concentrations of raindrops (≈ 3 mm) were obtained at the 1800 m level, at the border of the 50 dBZ core. At these higher altitudes, larger drops were very scarce as compared with those found at 1200 m height.

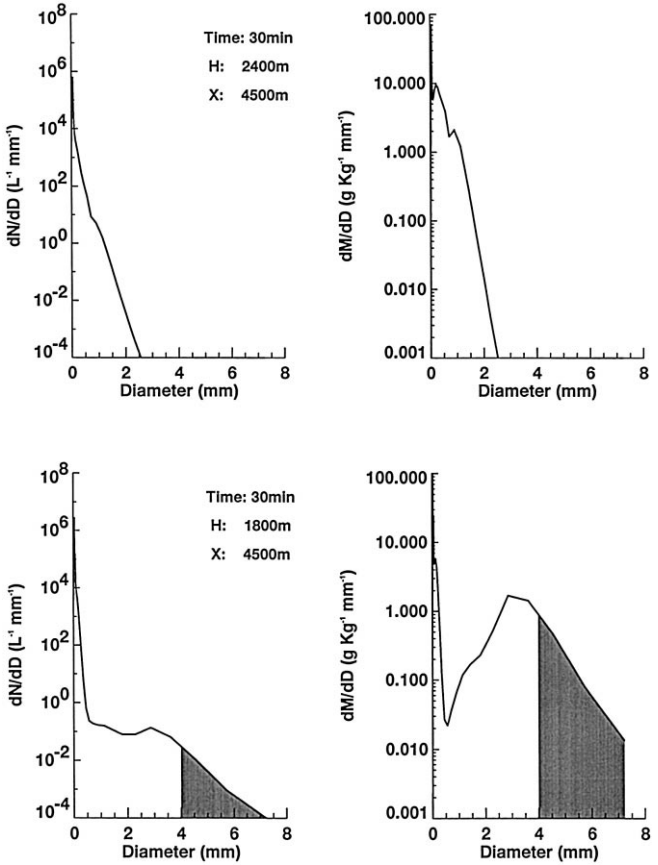

Fig. 7. As in Fig. 6, at a height of 1800 m (lower graphs) and 2400 m (upper graphs).

In the upper part of the cloud (2400 m), the giant drops were completely absent because the updrafts were too weak (≈ 3.5 m s^{-1}) to lift or levitate them.

Fig. 8 shows the distribution functions at the center of the domain and at 1200 m height, 25 and 35 min from model initiation. At 25 min, the first few giant drops began to appear. At 35 min, the radar reflectivity decreased from ≈ 60 dBZ to ≈ 50 dBZ and, as the distributions show, the number and mass of the giant drops decreased as compared to those shown in Fig. 6. During the same period of time, the number and mass of raindrops in the range of 1–3 mm increased, suggesting that the presence of small raindrops enhanced the probability for binary breakup, thus decreasing the formation of giant drops. This point will be further discussed later. Fig. 9 presents the distribution functions at 1200 m height and 30 min of cloud simulation, 200 and 400 m away from the domain center. As can be seen, the number of giant drops (> 4 mm) decreased away from the center of the domain, while the number of smaller raindrops (< 4 mm) increased.

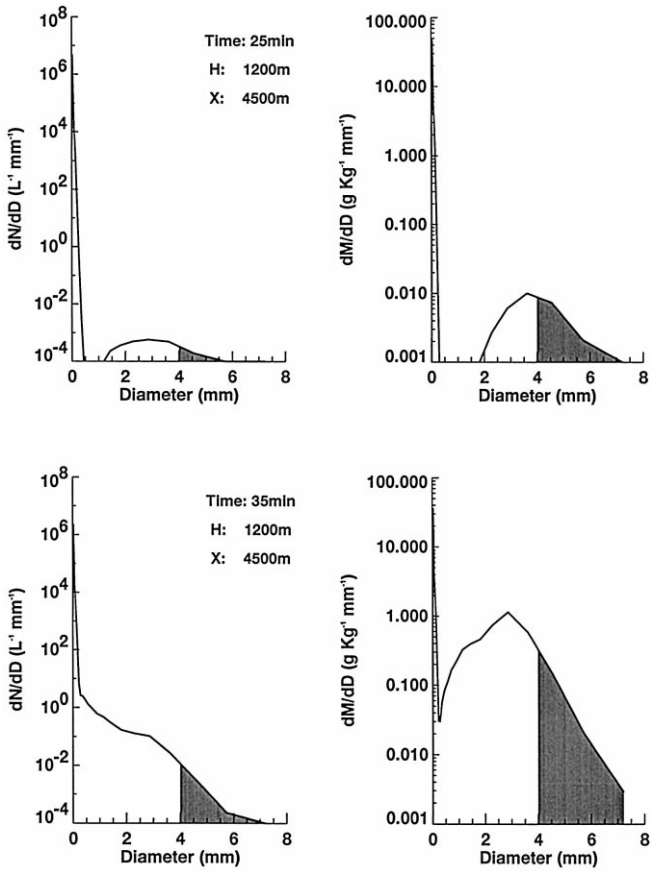

Fig. 8. Size distributions by number and mass, 25 min (lower graphs) and 30 min (upper graphs) min from model initiation at domain center, at a height of 1200 m.

4.1. The role of the initial drop spectra

The influence of the shape of the initial drop spectra resulting from the nucleation of CCN on the development of the precipitation and of the high-reflectivity cores was tested. The Reference case, described before, represents the case in which a broad gamma function was used with a relatively large average radius. Case A represented a test in which droplets formed by nucleation on CCN were inserted into the first bin, with an average mass corresponding to the middle of the bin. Case B was a test using the same shape parameters of the gamma function as in the Reference case, but with a smaller average radius (7 μm).

In general, the main effect of changing the initial drop spectra was in the time required to initiate the collision–coalescence process and the formation of raindrops. Fig. 10 shows the radar reflectivity at the center of the domain for cases A and B. By comparing Figs. 4 and 10 it can be seen that the wide initial distribution in the Reference

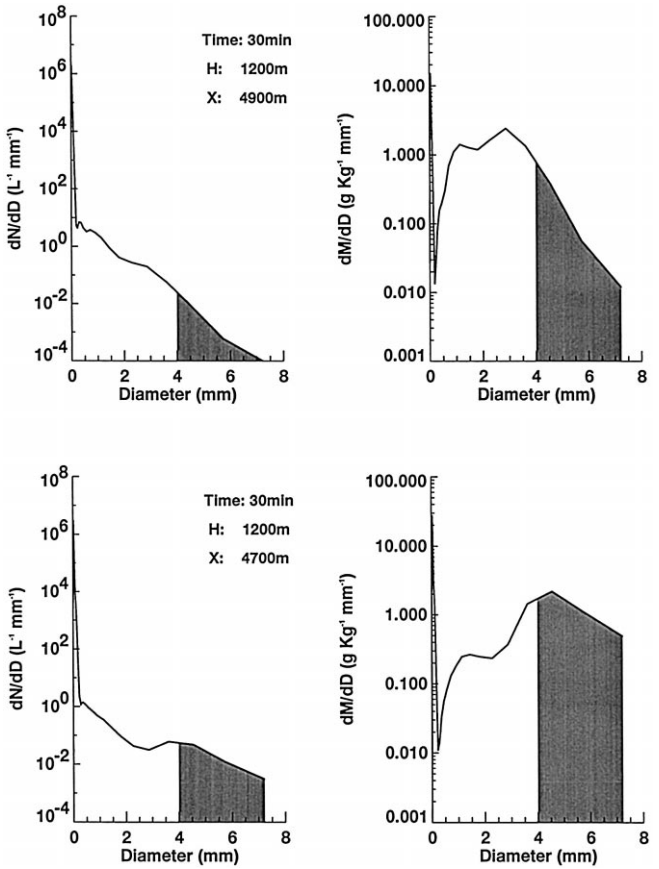

Fig. 9. Size distributions by number and mass, 30 min from model initiation at a height of 1200 m and at two distances from the center of the domain (located at 4500 m)—200 m (lower graphs) and 400 m (upper graphs).

case, rapidly developed raindrops so that the 10 dBZ contour reached the surface after 26 min, 2 min before case B and 6 min earlier than case A. In spite of the delay in the development of the first echoes in case A, once the first raindrops appeared, the subsequent growth was very fast, as can be seen from the strong gradient of the radar reflectivity contours in comparison to those in Fig. 4 for the Reference case. The maximum radar reflectivity in the three cases was reached at almost the same time, $\approx$ 32 min from model initiation, with small differences in the actual values obtained 57.3–62.2 dBZ. As will be discussed later, the results obtained in case B show the best comparisons with the measurements in terms of the rate of development of radar reflectivities.

Distribution functions for cases A and B are shown in Fig. 11 for the same time and location (close to the maximum radar reflectivity). In both cases, the large end of the spectrum was similar, the differences mainly appeared for raindrops with diameters

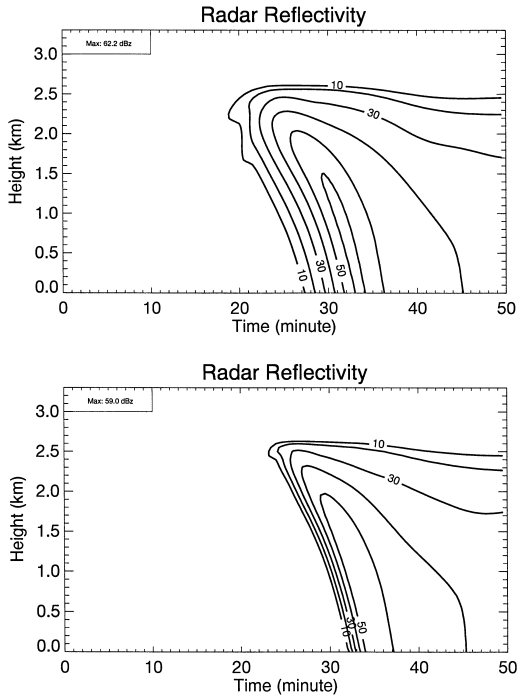

Fig. 10. Radar reflectivity (in dBZ) as a function of height and time, averaged over 50 m, at the center of the domain for case A (bottom) and B (top).

between ≈ 0.5–3 mm. The number and mass concentrations of drops in this size range in case A were significantly smaller than in B.

4.2. The role of the breakup processes

The model used in these simulations is the only one we know of that simulates breakup of drops as a result of collisions using Low and List kernels (Low and List, 1982a,b). Most of the models use spontaneous breakup as the only mechanism that limits the growth of the drops. In principle, these two processes may occur simultaneously, although their probabilities are much different (as already stated, spontaneous breakup seems to be very rare in nature, e.g. Rogers and Yau, 1989). Also important, especially in the present simulations, is the fact that while spontaneous breakup always result in fragments smaller than the parent drops, binary breakup results in fragments that one of them is larger than either of the colliding drops. Therefore, although binary breakup starts earlier when the drops are smaller, it can generate larger drops in the process.

Three simulations were conducted in addition to the Reference case. In the first one (C) both spontaneous and binary breakup were included. In case D, only spontaneous breakup was considered, and in the third one (E) no breakup process was included. In all cases, the same initial cloud drop distributions were used. Fig. 12 presents the radar

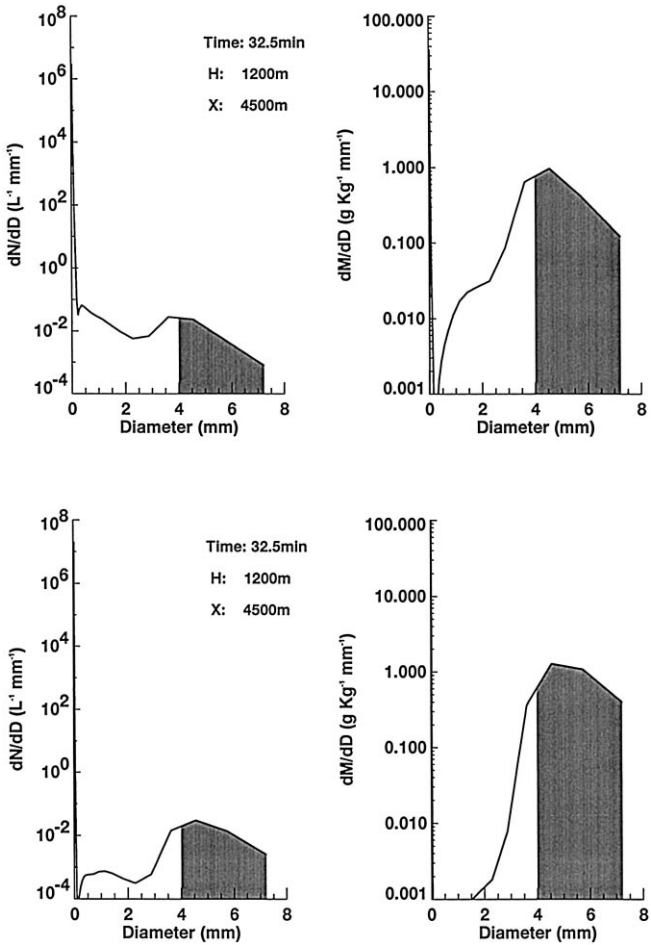

Fig. 11. Size distributions by number and mass, 32.5 min from model initiation at the center of the domain, at a height of 1200 m for case A (lower graphs) and B (upper graphs).

reflectivity at the domain center as a function of time for cases C and D. No significant differences appear among the three cases (Reference, C and D) until 20 min from model initiation. In case C, the development of the spectra was similar to the Reference case (see Fig. 4), except that the spontaneous breakup significantly reduced the number of giant drops and consequently reduced the radar reflectivity. For this reason, the rate of increase of the radar reflectivity was reduced, and a maximum radar reflectivity of only 55.1 dBZ was reached 1–2 min earlier than in the Reference case (61.4 dBZ). In the Reference and C cases, the maximum LWC and rain rate were very similar.

The development of the cloud in case D was significantly different. Due to the absence of binary breakup drops could reach larger sizes. The effect of the spontaneous breakup becomes significant ($> 0.1\ s^{-1}$) only for drops larger than 3.7 mm. Echoes of

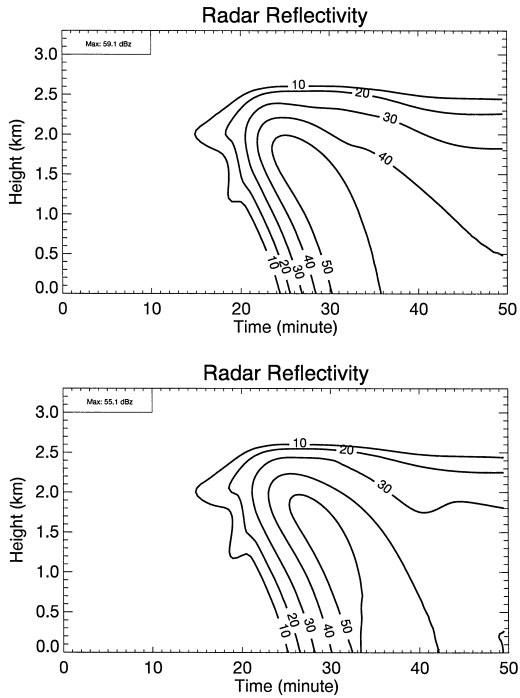

Fig. 12. Radar reflectivity (in dBZ) as a function of time and height, averaged over 50 m, at the center of the domain for case C (bottom) and D (top).

high reflectivity developed about 1 min earlier in D than in the Reference case. The bigger drops in case D began falling at an earlier stage and at a certain point began breaking up. Since in the kinematic model the microphysical processes did not affect the dynamics, the giant drops that descended, encountered large amounts of LWC in the persisting strong updrafts. Fig. 13 shows contours of LWC for the Reference and D cases, 25 and 30 min from model initiation. As already stated, case D produced larger drops that began falling against the updrafts at an earlier stage. At 25 min, the updrafts reached their maximum value (8 m s^{-1}, see Fig. 1) and drops smaller than ≈ 3 mm were suspended or levitated while growing by collection of smaller drops supplied by the ascending air. This growth produced a high reflectivity core with a maximum LWC of 5.24 g kg^{-1}. In the Reference case, the drops grew slower allowing the outflow near cloud top to move these drops away from the main updraft (see the 2 g kg^{-1} contour in the two cases). In this case the maximum LWC was smaller and it was located at a higher altitude, above the maximum updraft, thus reducing the intensity of the echo. At 30 min the maximum LWC in case D increased up to 7.5 g kg^{-1}, while in the Reference case, it was only 4.75 g kg^{-1}. Here again, it can be seen that the region of high LWC is broader in the Reference case than in D (e.g., 1 g kg^{-1} contour).

A closer look at the drop spectra reveals other effects produced by spontaneous breakup. Fig. 14 shows the mass and number distribution functions, 30 min from model

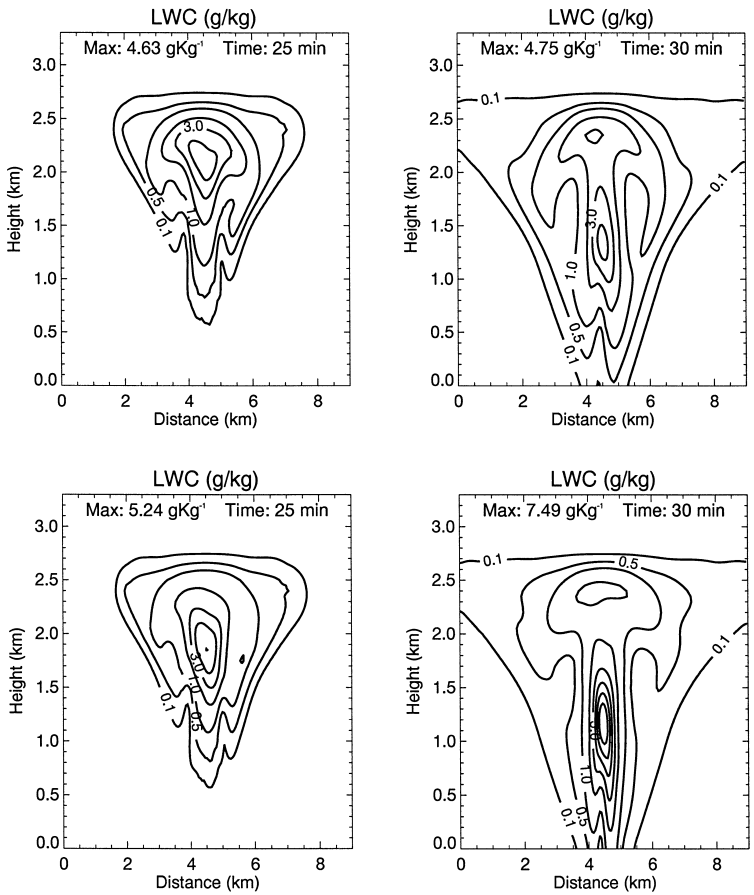

Fig. 13. Contours of LWC at 25 and 30 min from model initiation for the Reference case (top) and case D (bottom).

initiation at a height of 1200 m, and at the center of the domain. The lower plots represent case C and the top ones case D. When comparing these two plots with the Reference case (Fig. 6, top) two things become clear. Spontaneous breakup produced fewer drops larger than ≈ 5 mm than in the Reference case. The number of drops in the range 0.5–4 mm was much larger than when spontaneous breakup was not active. The lack of giant drops was a result of the relatively high probability of spontaneous breakup according to Komabayasi et al. (1964) (about 1 s^{-1} for this size drops). The larger number of drops in the 0.5–4 mm range was due to the large number of fragments produced by spontaneous breakup in comparison to binary breakup (62.2 per event in contrast to 3–5 per collision when using Low and List kernels). The ratio of the number of giant drops (> 4 mm) to the total number of raindrops (> 0.5 mm) was 0.8 in the Reference case (Fig. 6, top), 0.0424 in case C and 0.084 in case D (Fig. 14, bottom and top, respectively). This indicates that spontaneous breakup considerably reduced the

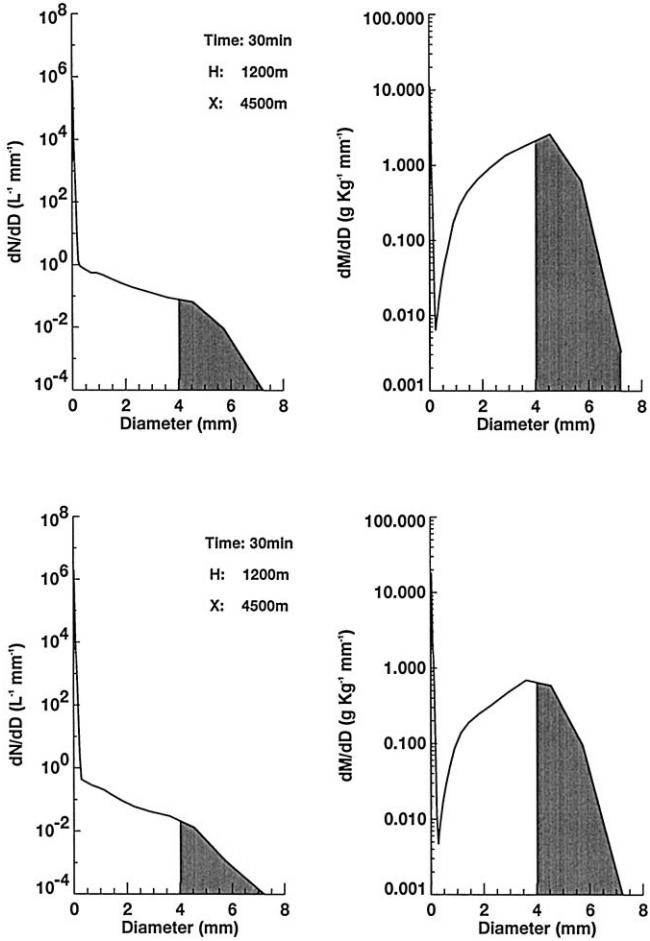

Fig. 14. Size distributions by number and mass, 30 min from model initiation at the center of the domain, at a height of 1200 m for case C (lower graphs) and D (upper graphs).

number of giants drops and increased the number of smaller raindrops. It should be pointed out that because of the reasons stated above, the LWC and number concentration at this time (30 min) and location (1200 m height and center of domain) was larger by a factor of 2 in D than in C.

In case E, no breakup mechanisms were included. The physical meaning is that drops that collide, and according to Low and List kernel should breakup, in this case just bounce (elastic collision). In other words, in the present case, drops grew by accretion, but did not breakup. The results obtained here revealed that the number and mass concentrations of the giant drops and raindrops in the range 1.5–2.5 mm were significantly smaller than in the Reference case. This can be seen in Fig. 15 that displays the drop spectra (number and mass concentration) for the Reference and E cases at the

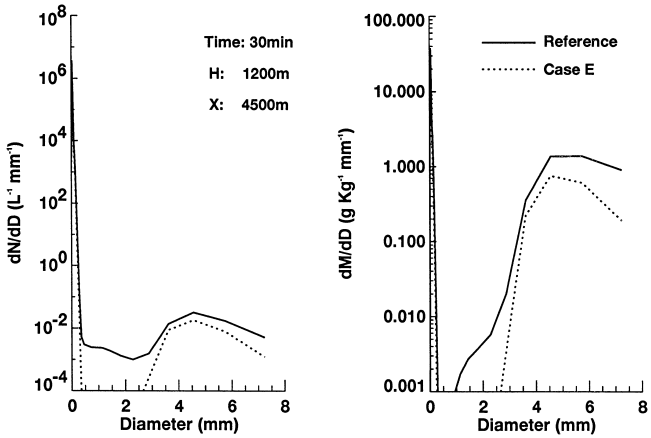

Fig. 15. Size distributions by number and mass, 30 min from model initiation at the center of the domain, at a height of 1200 m for the Reference case (solid line) and case E (dotted line).

center of the domain, at a height of 1200 m, 30 min from model initiation. Also, the number of giant drops were smaller than in the Reference case in which binary breakup was included. This surprising result could be easily explained by the fragment distribution in the Low and List kernel formulation. According to the breakup probabilities of Low and List, collision of drop pair larger than 3 mm and 1 mm will produce fragments such that the largest one will be larger than either of the parent drops. In other words, drops larger than 3 mm in diameter will be produced. By suppressing the binary breakup, we actually reduced the number of giant drops and also decreased the number of smaller fragments created in the breakup event. This important point will be further discussed Section 5.

5. Discussion

In spite of the limitations of a 2D cloud model to accurately describe a natural cloud, and the inaccuracies in radar and drop spectra measurements, some useful comparisons could be made in order to validate the numerical model, and to help explain some of the observations. The results from the numerical simulations can be compared with the observations reported by Szumowski et al. (1997a,b) (hereafter S1 and S2, respectively). Fig. 15 in the paper by S1 presents the maximum radar reflectivity and its height as a function of time for the August 10th event. By comparing this data with that obtained in the Reference, A and B cases, an evaluation of the model performance can be obtained. Since no information on the initial droplets spectra of the cloud is available, it may be inferred by matching the simulated development of the reflectivity cores with the radar observations.

Fig. 16 presents the maximum radar reflectivity and its height as a function of time for the Reference, A and B cases. Case B seems to be the one that presents the closest

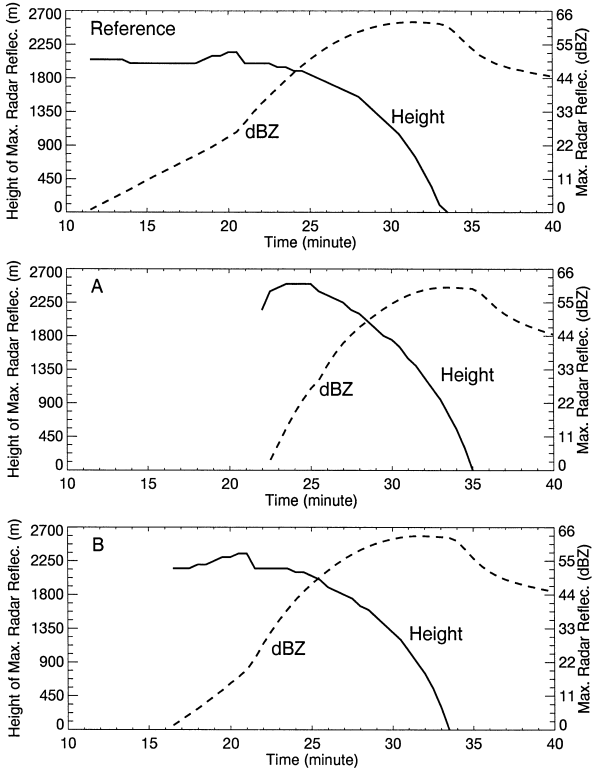

Fig. 16. The height and intensity (dBZ) of the maximum radar reflectivity at the center of the domain as a function of time for the Reference, A and B cases.

resemblance to the observations. In case B, 15 min elapsed between the appearance of the 0 dBZ echo and the maximum reflectivity. According to the observations, this time was ≈ 17 min. The maximum reflectivity was 60 dBZ in the measurements as compared to 62 dBZ in case B. Although in the model, the first echo appeared at a higher level than in the observations, it succeeded to reproduce the height of the maximum reflectivity, some 5 min after the appearance of the 0 dBZ echo. Also, in the model, once the high reflectivity cores developed, they descended faster than in the measurements. Possible reasons for the differences are that the kinematic model did not exactly reproduce the dynamical fields that existed during the measurements, and that the actual initial drop spectrum was different from that used in the simulations.

The development of the radar reflectivity was fairly well reproduced by the model, including the fact that after reaching the maximum reflectivity, its value remained constant for a few minutes while its location descended toward the surface. The rate of increase of the maximum radar reflectivity was somewhat different in the observations and in the numerical simulations. Fig. 16 shows that when the initial drop spectrum was broader (Reference and case B), the high reflectivity zones developed earlier and at a

lower elevation. In these two cases, the growth was moderate during the first few minutes, before the cloud reached its maximum updraft, and accelerated afterwards. When the initial drop spectrum was wide, large drops formed by collection as they ascended. When they reached the higher levels of the cloud, those that were big enough to overcome the updrafts, precipitated. When the updrafts gradually increased, a larger number of large drops could be levitated as well, leading to a gradual increase in radar reflectivity. At the maximum updrafts, most of the large drops were sustained, and they continued growing by collection of smaller drops ascending in the updraft. At this stage, the growth of the maximum radar reflectivity accelerated. Comparing Figs. 1 and 16 can be seen that the rapid increase in radar reflectivity occurring at 21–22 min from model initiation, when the updrafts reached their maximum value. In case A, no large drops could grow during the ascension, and they formed only at the top of the maximum updrafts. In the observations, the rate of increase of the radar reflectivity was higher at the first stages of the echo formation, suggesting that the actual initial drop spectra could be narrower than the one used in case B, but with a small tail representing a few giant CCN. Such initial drop spectra could trigger the early growth of some of the drops and lead to the same radar echo development as observed.

The model also succeeded in reproducing the narrow columns in which the high reflectivity cores developed (≈ 800 m, see Fig. 5a,b) and the high gradient of radar reflectivity close to cloud top.

Observations of drop spectra were presented by S2. Although their measurements were not conducted on the same day as the radar observations, the feeling was that the two cases were very similar (S2), and that at least qualitatively, the drop spectra on the two days were similar. Drop spectra presented by S2 show in some cases tens of drops with diameters larger than 4 mm. In these cases, the measured radar reflectivities were larger than 50 dBZ. The results shown in Figs. 6, 8 and 9 for the simulated drop spectra at the region of high radar reflectivities, resemble the observations in S2, in terms of spectral shape, number of giant drops and maximum size obtained by the drops.

In order to explain the formation of the giant drops, S2 argue that the relatively strong and stable updraft in the cloud helped sort out between small and big raindrops according to their terminal velocities. Therefore, the big raindrops fell through a region in which most of the smaller raindrops had been advected away. As a result, the probability of breakup through collision with small raindrops was low, while at the same time these drops continued to grow by accretion of cloud droplets. The results of the present model seem to confirm this hypothesis. This can be seen in Fig. 6 where the drop spectra at the center of the domain, at the location of the high-reflectivity echos, shows a low concentration of small raindrops. In these cases, the number of breakup events produced by collision was indeed very low.

Another process that also contributes to the formation of giant drops is the collision and breakup of large raindrops. According to the kernel of Low and List, a fragment larger than any of the colliding drops can be created in such binary collisions. Case E, in which no breakup processes were included, confirms this point. In this case, the giant drops were created only through accretion of small droplets by raindrops, as described above. Although growth by accretion can produce giant raindrops, their concentrations are lower than in the case when both accretion and binary breakup are included.

The simulations that included spontaneous breakup, did not succeed in reproducing some of the key features presented in S2. The development of giant drops, as appeared in the observations, was almost absent in the simulations (Fig. 14). Also, spontaneous breakup significantly increased the number of small raindrops, because of the formulation of the distribution function of the fragments. Such concentrations of small raindrops were not observed.

6. Conclusions

The development of high-reflectivity cores and the formation of giant drops were simulated using a kinematic model with detailed formulation of the microphysical processes. The results were compared with observations and were found to satisfactorily reproduce the radar reflectivity fields and drop spectra.

The rate of development of rain and radar echoes varied with different initial drop spectra. Using a broad initial drop spectrum with a large average radius advanced the initiation of the collision–coalescence process, and raindrops were produced very rapidly. In contrast, a very narrow drop spectrum with a small average radius required a longer time to produce the first raindrops. In spite of that, the maximum radar echoes and the size spectra in these cases were similar. Results obtained with a relatively broad initial drops spectra and average radius of 7 μm yielded the closest resemblance to the observations.

Our results show that drop breakup mechanisms are key to the understanding of the formation of giant drops. The airflow in the kinematic model used here sorted out drops based on their fall velocities. Consequently, millimeter size drops descended through a cloud of smaller drops. Collisions between these falling raindrops and the cloud droplets did not lead to breakup and helped produce giant raindrops ($D > 4$ mm). Binary collisional breakup of big raindrops also played a significant role in the formation of giant drops. Only when binary breakup was the sole active breakup process did giant drops develop in concentrations similar to those observed.

Spontaneous breakup occurs very rarely in nature and only under extreme conditions, while binary breakup is a much more common process. Spontaneous breakup (with or without binary breakup) restricted the formation of giant drops. In this case, the drop spectra reported in the measurements could not be explained. Since most numerical models of clouds only include spontaneous breakup, it could be concluded that only binary breakup (and not spontaneous breakup) mechanism should be used in numerical simulations of warm rain formation.

Acknowledgements

Part of this work was supported by the Water Commissioner of Israel under the Rain Enhancement Project. Thanks are also due to Mrs. and Mr. L. Ross for their contribution to the laboratory, which made part of this work possible. Comments by one of reviewers (B) helped us clarify some important points. We thank him/her for that.

References

Beard, K.V., 1977. Terminal velocity adjustment for cloud and precipitation. J. Atmos. Sci. 33, 851–864.
Beard, K.V., Johnson, D.B., Baumgardner, D., 1986. Aircraft observations of large raindrops in warm, shallow, convective clouds. Geophys. Res. Lett. 19, 991–994.
Feingold, G., Tzivion, S., Levin, Z., 1988. The evolution of raindrop spectra: Part I. Stochastic collection and breakup. J. Atmos. Sci. 45, 3387–3399.
Kogan, Y.L., 1991. The simulation of a convective cloud in a 3-d model with explicit microphysics: Part I. Model description and sensitivity experiments. J. Atmos. Sci. 48, 1160–1189.
Komabayasi, M., Gonda, T., Isono, K., 1964. Lifetime of water drops before breaking and size distribution of fragment droplets. J. Meteor. Soc. Jpn. 42, 330–340.
Lavoie, R.L., 1967. Background data for the warm rain project. Tellus 19, 348–353.
Long, A.B., 1974. Solutions to the droplet coalescence equation for polynomial kernels. J. Atmos. Sci. 11, 1040–1057.
Low, T.B., List, R., 1982a. Collision coalescence and breakup of raindrops: Part I. Experimentally established coalescence efficiencies and fragments size distribution in breakup. J. Atmos. Sci. 39, 1591–1606.
Low, T.B., List, R., 1982b. Collision coalescence and breakup of raindrops: Part II. Parameterization of fragment size distributions in breakup. J. Atmos. Sci. 39, 1607–1618.
Ochs, H.T., Czys, R.R., Beard, K.V., 1986. Laboratory measurements of coalescence efficiencies for small precipitating drops. J. Atmos. Sci. 43, 225–232.
Pontikis, C., Isaka, H., Jochum, A., Jonas, P., Schaller, E., 1987. Meeting review: workshop on warm convective clouds, 9–10 February 1987, Paris, France. Bull. Am. Meteor. Soc. 68, 1254–1256.
Pruppacher, H.R., Klett, J.D., 1997. Microphysics of Clouds and Precipitation. Kluwer Academic Pub., 954 pp.
Rauber, R.M., Beard, K.V., Andrews, B.M., 1991. A mechanism for giant raindrop formation in warm, shallow, convective clouds. J. Atmos. Sci. 48, 1791–1797.
Rogers, R.R., 1967. Doppler radar investigation of Hawaiian rain. Tellus 19, 433–455.
Rogers, R.R., Yau, M.K., 1989. A Short Course in Cloud Physics. Pergamon, 293 pp.
Smolarkiewicz, P.K., Rasmussen, R.M., Clark, T.L., 1988. On the dynamics of hawaiian cloud bands: island forcing. J. Atmos. Sci. 45, 1872–1905.
Srivastava, R.C., 1971. Size distribution of raindrops generated by breakup and coalescence. J. Atmos. Sci. 28, 410–415.
Stevens, B., Feingold, G., Cotton, W.R., Walko, R.L., 1996. Elements of the microphysical structure of non-precipitating numerically simulated stratocumulus. J. Atmos. Sci. 53, 980–1006.
Szumowski, M.J., Rauber, R.M., Ochs, H.T., Miller, L.J., 1997a. The microphysical structure and evolution of Hawaiian rainband clouds: Part I. Radar observations of rainbands containing high reflectivity core. J. Atmos. Sci., in press.
Szumowski, M.J., Rauber, R.M., Ochs, H.T., Beard, K.V., 1997b. The microphysical structure and evolution of Hawaiian rainband clouds: Part II. Microphysical measurements within rainbands containing high reflectivity cores. J. Atmos. Sci., in press.
Szumowski, M.J., Grabowski, W.W., Ochs, H.T., 1998. Simple two-dimensional kinematic framework designed to test warm rain microphysical models. Atmos. Res. 45, 299–326.
Takahashi, T., 1981. Warm rain development in a three-dimensional cloud model. J. Atmos. Sci. 38, 1991–2013.
Takahashi, T., Yoneyama, K., Tsubota, Y., 1989. Rain duration in Hawaiian trade wind rainbands—aircraft observation. J. Atmos. Sci. 46, 1773–1790.
Tzivion, S., Feingold, G., Levin, Z., 1987. An efficient numerical solution of the stochastic collection equation. J. Atmos. Sci. 44, 3139–3149.
Tzivion, S., Feingold, G., Levin, Z., 1989. The evolution of raindrop spectra: Part II. Collisional collection/breakup and evaporation in a rainshaft. J. Atmos. Sci. 46, 3312–3327.
Tzivion, S., Reisin, T., Levin, Z., 1994. Numerical simulations of hygroscopic seeding in a convective cloud. J. Appl. Meteor. 33, 252–267.